A Simple Model of Water and the Hydrophobic Effect

Kevin A. T. Silverstein,[†] A. D. J. Haymet,*[,‡] and Ken A. Dill*[,§]

Contribution from the Department of Pharmaceutical Chemistry and Graduate Group in Biophysics, University of California, San Francisco, California 94143-1204, and School of Chemistry, University of Sydney, NSW 2006, Australia

Received August 28, 1997. Revised Manuscript Received January 21, 1998

Abstract: We use a simple computational model, proposed originally by Ben-Naim, to study the anomalous properties of water and the hydrophobic effect. Water molecules are modeled as two-dimensional (2D) Lennard-Jones disks, with three orientation-dependent hydrogen-bonding arms, arranged as in the Mercedes Benz (MB) logo. Phase space is explored using NPT Monte Carlo simulations. For pure water, the MB model qualitatively predicts the density anomaly (and the related negative thermal expansion coefficient at low temperature), the minimum in the isothermal compressibility as a function of temperature, the large anomalous heat capacity, and freezing to the 2D model analogue of ice, a low-density hexagonal crystal phase. For the solvation of nonpolar solutes (disks without H bonds), the model predicts the experimental trends with temperature of the free energy, entropy, enthalpy, molar volume, and heat capacity. A unique feature of these simulations is that they provide well-converged heat capacities of transfer, an important fingerprint of hydrophobicity. This model gives an explanation for the temperature, T_S, at which the transfer entropy of nonpolar solutes is zero: below this temperature, shell water molecules have more hydrogen bonding than bulk water molecules; above T_S, the reverse is true.

1. Introduction

Water is regarded as an unusual and poorly understood liquid. Water properties have been reviewed extensively in the literature.[1−6] Relative to simpler liquids, water has certain anomalous thermodynamic properties: a temperature of maximum density in the liquid phase over a wide range of pressures, an unusually high surface tension, a minimum in the isothermal compressibility as a function of temperature, and a large heat capacity throughout the liquid range. These properties are thought to arise from the ability of water to form tetrahedrally coordinated hydrogen bonds. There remains vigorous debate, however, over the role of hydrogen bonding in the properties of liquid water.[2,3,6]

Water is also unusual as a solvent, particularly for nonpolar solute molecules.[4,7−10] Unlike simpler solvents, the insertion of nonpolar solutes into water is (1) strongly unfavorable, (2) strongly opposed by entropy at room temperature, and (3) accompanied by a large positive heat capacity. These properties define the hydrophobic effect.

The physical basis for the hydrophobic effect has been the subject of debate. One group[10−14] holds that the large aversion of oil for water results mostly from the small size of the water molecule, and not from water structuring by the solute. This conclusion arose out of the surprising success of the scaled particle theory[15] (SPT) to account for the free energy of hydrophobic transfers.[12,16] The proponents of this hypothesis argue that the entropic and enthalpic contributions arising from the structuring of water molecules largely compensate each other. Hence, they suggest that "structural reorganization is of little importance".[14] Others believe that the large positive heat capacity of insertion of nonpolar solutes is a defining feature of hydrophobicity, and that it results from hydrogen bonding and the ordering of water molecules around the solute. SPT cannot account for this key element.[13,14] The key issue is whether the free energy is sufficient to characterize hydrophobicity, or whether other thermodynamic derivatives are equally important, and more revealing. It is our belief that the free energy alone masks the underlying physics, and fails to provide predictive power for more complex situations (such as size, shape, and multiple-body effects). Structural details and mechanisms must be understood before further predictions can be made on these systems.

* To whom correspondence should be addressed.
[†] Graduate Group in Biophysics. Present address: Department of Chemistry, University of Minnesota, Minneapolis, Minnesota 55455.
[‡] University of Sydney. Present address: Department of Chemistry and Institute for Molecular Design, University of Houston, Texas 77204.
[§] Department of Pharmaceutical Chemistry.

(1) Eisenberg, D.; Kauzmann, W. *The structure and properties of water*; Oxford University Press: Oxford, 1969.
(2) Franks, F., Ed. *Water, a Comprehensive Treatise*; Plenum Press: New York, 1972−1982; Vol. 1-7.
(3) Stillinger, F. H. *Science* **1980**, *209*, 451−457.
(4) Tanford, C. *The Hydrophobic Effect: formation of micelles and biological membranes*, 2nd ed.; Wiley: New York, 1980.
(5) Zhu, S.-B.; Singh, S.; Robinson, G. W. *Adv. Chem. Phys.* **1994**, *85*, 627−731.
(6) Robinson, G.; Zhu, S.-B.; Singh, S.; Evans, M. *Water in Biology, Chemistry and Physics: Experimental Overviews and Computational Methodologies;* World Scientific: Singapore, 1996.
(7) Frank, H. S.; Evans, M. W. *J. Chem. Phys.* **1945**, *13*, 507.
(8) Ben-Naim, A. *Hydrophobic Interactions;* Plenum Press: New York, 1980.
(9) Privalov, P. L.; Gill, S. J. *Adv. Protein Chem.* **1988**, *39*, 191−234.
(10) Blokzijl, W.; Engberts, J. B. F. N. *Angew. Chem., Int. Ed. Engl.* **1993**, *32*, 1545−1579.
(11) Lee, B. *Biopolymers* **1985**, *24*, 813−823.
(12) Soda, K. *J. Phys. Soc. Jpn.* **1989**, *58*, 8643−4649.
(13) Lee, B. *Biopolymers* **1991**, *31*, 993−1008.
(14) Soda, K. *J. Phys. Soc. Jpn.* **1993**, *62*, 1782−1793.
(15) Pierotti, R. A. *Chem. Rev.* **1976**, *76*, 717.
(16) Postma, J. P. M.; Berendsen, H. J. C.; Haak, J. R. *Faraday Symp. Chem. Soc.* **1982**, *17*, 55−67.

S0002-7863(97)03029-1 CCC: $15.00
Published on Web 03/19/1998

To provide a physical explanation for the properties of water and the hydrophobic effect, many simulation models have been developed over the years.[17−22] These traditional simulation models usually aim for realism in representing the geometric structure of water. But there are two intrinsic limitations of an atomistically accurate, three-dimensional model of water. First, such models require large computational investments, and some properties—particularly those involving multiple derivatives of the free energy—are computationally prohibitive to study directly, such as the heat capacity of transfer. Yet this is precisely the property that is considered a "signature" of the hydrophobic interaction.[23−25] Second, simplified models can often address questions of principle that cannot be addressed in more realistic models. Realistic models tend to include many variables, geometric details, and types of interactions, including electrostatics, dipoles, hydrogen bonding, and van der Waals interactions. In simpler models, with fewer parameters, it is easier to ascertain the dominant interactions, and to trace the connection from assumptions about driving forces to the observable properties.

Our aim here is to develop a simplified model, with the details stripped away. We want to see how much of the behavior of pure water, and of the hydrophobic effect, is simply due to a balance between Lennard-Jones interactions and orientation-dependent hydrogen bonding. No other electrostatic terms are included explicitly. Our aim is a simplest "toy" model of the physics, not a most-realistic model of the geometry. We use a two-dimensional model. Its limitations are that it gives up atomic structural detail, and three-dimensionality, but it uses only a few parameters, and is computationally simple enough to explore properties that are difficult to study in more realistic models.

The two-dimensional model that we explore is one of a family of models first introduced by Ben-Naim[26] in 1971. He investigated the structure of the pure fluid[26,27] and a dilute hydrophobic solution[28,29] using an integral equation formalism. Then, he explored several parameter sets using NVT Monte Carlo simulations at a single phase point for each parametrization, and obtained more accurate distributions of the pure fluid.[30] Concurrently, more realistic 3D models were being developed.[17,18] Consequently, the Ben-Naim model was all but neglected until recently when Andaloro and Sperandeo-Mineo showed that it was simple enough to teach students about hydrophobicity without high-powered computers.[31] Andaloro and Sperandeo-Mineo explored a wider range of structural features of this model fluid around a fixed inert solute,[31] and showed enhanced local structuring. Although their simulations were not well converged, they nonetheless showed that the model gives useful insights.

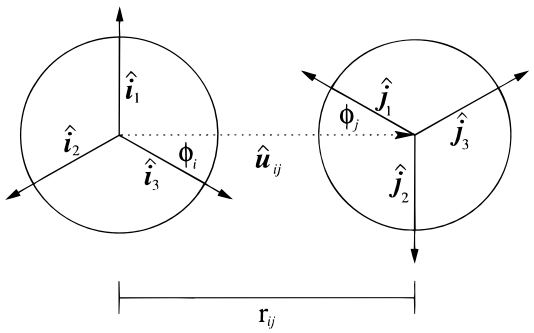

Figure 1. Two representative MB water molecules with indices *i* and *j*, separated by a distance r_{ij}. Each molecule has three hydrogen bonding arm vectors: $\hat{\boldsymbol{i}}_k$ and $\hat{\boldsymbol{j}}_l$, respectively (k, $l = 1, 2, 3$). The intermolecular axis vector is denoted $\hat{\boldsymbol{u}}_{ij}$ and the angles that the closest arm of each molecule make with this vector are labeled ϕ_i and ϕ_j.

To date, what has *not* been explored in this model are effects of temperature and pressure, or thermal properties other than the internal energy. Many other 3D simulations are similarly limited. Pair correlation functions and counts of hydrogen bonds converge quickly, but the calculation of the transfer thermodynamics is quite expensive computationally. The computational requirements of the 3D models make systematic studies of solvation extremely difficult. With a simplified model, however, we can study systematically here the link between microscopic structures and the macroscopic thermodynamics.

The present paper shows that LJ and orientation-dependent hydrogen bonding are sufficient, even in a 2D model, to capture a remarkably broad range of the experimentally observed thermodynamic properties of pure water and the hydrophobic effect. Many of the results are consistent with more realistic simulations.[32,33]

This paper is organized as follows. In Section 2, we define the MB model, briefly reviewing others of similar philosophy. Section 3 contains a description of the computational methods used. Then, in Sections 4 and 5, we compare our computed thermodynamic trends with those of experiments on bulk water and nonpolar solutions, respectively. Section 6 is a summary.

2. Model Description

Waters are represented in this model as two-dimensional disks with three symmetrically arranged arms, separated by an angle of 120°, as in the Mercedes Benz logo. Molecules interact pairwise through a Lennard-Jones (LJ) term and an explicit hydrogen-bonding (HB) term,

$$U(\boldsymbol{X}_i,\boldsymbol{X}_j) = U_{\mathrm{LJ}}(r_{ij}) + U_{\mathrm{HB}}(\boldsymbol{X}_i,\mathbf{X}_j) \qquad (1)$$

We use Ben-Naim's notation, summarized in Figure 1: $\boldsymbol{X}_i$ denotes the vector representing both the coordinates and the orientation of the *i*th particle, and r_{ij} is the distance between the molecular centers of particles *i* and *j*. The LJ term is defined in the usual fashion

(17) Stillinger, F. H.; Rahman, A. *J. Chem. Phys.* **1972**, *57*, 1281−1292.
(18) Stillinger, F. H.; Rahman, A. *J. Chem. Phys.* **1974**, *60*, 1545−1557.
(19) Matsuoka, O.; Clementi, E.; Yoshimine, M. *J. Chem. Phys.* **1976**, *64*, 1351−1361.
(20) Berendsen, H. J. C.; Postma, J. P. M.; van Gunsteren, W. F.; Hermans, J. In *Intermolecular Forces;* Pullmann, B., Ed.; Reidel: Dordrecht, 1981.
(21) Jorgensen, W. L. *J. Chem. Phys.* **1982**, *77*, 4156−4163.
(22) Berendsen, H. J. C.; Grigera, J. R.; Straatsma, T. P. *J. Phys. Chem.* **1987**, *91*, 6269−6271.
(23) Dill, K. A. *Biochemistry* **1990**, *29*, 7133−7155.
(24) Gill, S. J.; Dec, S. F.; Olofsson, G.; Wadso, I. *J. Phys. Chem.* **1985**, *89*, 3758−3761.
(25) Muller, N. *Acc. Chem. Res.* **1990**, *23*, 23−28.
(26) Ben-Naim, A. *J. Chem. Phys.* **1971**, *54*, 3682−3695.
(27) Ben-Naim, A. *Mol. Phys.* **1972**, *24*, 705−721.
(28) Ben-Naim, A. *Chem. Phys. Lett.* **1971**, *11*, 389−392.
(29) Ben-Naim, A. *Mol. Phys.* **1972**, *24*, 723−733.
(30) Ben-Naim, A. *J. Chem. Phys.* **1973**, *59*, 6535−6555.
(31) Andaloro, G.; Sperandeo-Mineo, R. M. *Eur. J. Phys.* **1990**, *11*, 275−282.

(32) Preliminary results from this work have been reported at the International Symposium on Molecular Thermodynamics and Molecular Simulation in Japan.[33]
(33) Haymet, A. D. J.; Silverstein, K. A. T.; Dill, K. A. Hydrophobicity. In *International Symposium on Molecular Thermodynamics and Molecular Simulation*; Hosei University: Tokyo, Japan, 1997.

$$U_{\mathrm{LJ}}(r_{ij}) = 4\epsilon_{\mathrm{LJ}}\left[\left(\frac{\sigma_{\mathrm{LJ}}}{r_{ij}}\right)^{12} - \left(\frac{\sigma_{\mathrm{LJ}}}{r_{ij}}\right)^{6}\right] \quad (2)$$

where ϵ_{LJ} and σ_{LJ} are the well-depth and contact parameters, respectively. Neighboring water molecules form explicit hydrogen bonds when the arm of one molecule aligns with the arm of another, with an energy that is a Gaussian function of separation and angle,

$$U_{\mathrm{HB}}(\boldsymbol{X_i},\boldsymbol{X_j}) = \epsilon_{\mathrm{HB}} G(r_{ij} - r_{\mathrm{HB}}) \sum_{k,l=1}^{3} G(\hat{\boldsymbol{\imath}}_k \cdot \hat{\boldsymbol{u}}_{ij} - 1) G(\hat{\boldsymbol{\jmath}}_l \cdot \hat{\boldsymbol{u}}_{ij} + 1) \quad (3)$$

where $G(x)$ is an unnormalized Gaussian function,

$$G(x) = \exp[-x^2/2\sigma^2] \quad (4)$$

The unit vector $\hat{\boldsymbol{\imath}}_k$ represents the kth arm of the ith particle ($k = 1, 2, 3$) and $\hat{\boldsymbol{u}}_{ij}$ is the unit vector joining the center of molecule i to the center of molecule j. The parameters $\epsilon_{\mathrm{HB}} = -1$ and $r_{\mathrm{HB}} = 1$ define the optimal hydrogen bond energy and bond length, respectively. By this definition, the strongest hydrogen bond occurs when one arm of one water is perfectly collinear with the arm of another water. We make no distinction between donors and acceptors; this contribution to the energy is just defined by the degree to which two arms line up. Angular deviations from this lowest-energy hydrogen bond have a Gaussian variation in energy, with a single width parameter used to attenuate the interaction. The same width parameter is used for both distance and angle deviations (although in principle, two separate width parameters could be used: one for hydrogen bond stretching; the other for bending). Figure 1 shows the definitions of the distances and angles between two model water molecules.

In total, there are five parameters. Ben-Naim explored several combinations of parameters, of which we chose one for this work. The interaction energy, ϵ_{LJ} is one-tenth of ϵ_{HB}, and the LJ contact distance is 0.7 that of r_{HB}. The width of the Gaussian $\sigma = 0.085$ was chosen to be small enough that a direct H bond is more favorable than a bifurcated H bond. All energies and temperatures will be reported in reduced units, normalized to the strength of the optimal hydrogen bond (e.g., $T^* = k_{\mathrm{B}}T/|\epsilon_{\mathrm{HB}}|$, $H^* = H/|\epsilon_{\mathrm{HB}}|$). Similarly, all distances are scaled by the length of an idealized hydrogen bond separation (e.g., $V^* = V/r_{\mathrm{HB}}{}^2$).

A. Comparison with Other Simple Models. A completely different two-dimensional model has been investigated by Okazaki, Nosé, Kataoka and Yamamoto,[34] who subsequently studied a three-dimensional model that was related to it.[35] The model of Okazaki et al. displays four anomalous behaviors of water: a temperature of maximum density, a minimum in the isothermal compressibility, a shift in the temperature dependence between isobars of the thermal expansion coefficient, and the singular properties of supercooled water. Our model differs from theirs in the H-bond geometry, and ours is simpler insofar as it lacks any long-range electrostatics. No analysis of the solvation properties of their model has been published, to our knowledge. The success of the MB model indicates that explicit electrostatics and the distinction between donors and acceptors are not the central components of the physics of hydrophobic hydration.

Yet another primitive model was explored by Dahl and Andersen;[36,37] it too captures several anomalous properties of liquid water. Their three-dimensional model used a hard-sphere reference with a double square-well hydrogen bond potential that is tetrahedrally coordinated. The thermodynamics were computed by a cluster expansion approximation. More recently, Nezbeda et al. have investigated the structural properties of related models,[38−40] comparing the solutions of several approximations with Monte Carlo simulations. These authors used the model to investigate the phase behavior of inert gases and *n*-alkanes.[41,42] These models, like the one we explore, neglect the long-range Coulombic interactions and model the H-bonding explicitly. Simulations of these three-dimensional models are still reasonably expensive; hence the thermodynamics are only accessible through the approximate theories.

Among other recent, simplified 3D models of water are those based on an orientational octupole−octupole interaction.[43−46] These octupolar models, which have been developed by Blum and co-workers, have few parameters, and can be solved analytically, but are more or less still in the development stage. Lattice models of water have been studied by various researchers,[47−51] based upon the model of Bell.[52] In these models, waters are configured on a bcc lattice with a discrete number of orientational states, and the thermodynamics is often solved by a zeroth- or first-order approximation. These models have also been able to capture numerous anomalous properties of water, but the confines of the lattice may be too restrictive to correctly model the qualitative trends of hydrophobicity.[51]

3. Simulation Methods

A. General Procedure. To obtain thermodynamic and structural properties of MB water, we performed Monte Carlo simulations in the NPT ensemble.[53] At each successive step, a move for one molecule is chosen randomly among the following three options:

$$x \rightarrow x + \xi_1\Delta x, \qquad y \rightarrow y + \xi_2\Delta y, \qquad \phi \rightarrow \phi + \xi_3\Delta\phi \quad (5)$$

where the ξ_i's are random numbers generated over the interval $-1 \le \xi_i \le 1$, and Δx, Δy, and $\Delta\phi$ are fixed maximum

(34) Okazaki, K.; Nosé, S.; Kataoka, Y.; Yamamoto, T. *J. Chem. Phys.* **1981**, *75*, 5864−5874.
(35) Kataoka, Y.; Hamada, H.; Nosé, S.; Yamamoto, T. *J. Chem. Phys.* **1982**, *77*, 5699−5709.
(36) Dahl, L. W.; Andersen, H. C. *J. Chem. Phys.* **1983**, *78*, 1962−1979.
(37) Dahl, L. W.; Andersen, H. C. *J. Chem. Phys.* **1983**, *78*, 1980−1993.
(38) Kolafa, J.; Nezbeda, I. *Mol. Phys.* **1987**, *61*, 161−175.
(39) Nezbeda, I.; Iglesias-Silva, G. A. *Mol. Phys.* **1990**, *69*, 767−774.
(40) Nezbeda, I.; Slovák, J. *Mol. Phys.* **1997**, *90*, 353−372.
(41) Nezbeda, I.; Smith, W. R.; Kolafa, J. *J. Chem. Phys.* **1994**, *100*, 2191−2201.
(42) Nezbeda, I.; Kolafa, J.; Pavlíček, J.; Smith, W. R. *J. Chem. Phys.* **1995**, *102*, 9638−9646.
(43) Blum, L.; Vericat, F.; Bratko, D. *J. Chem. Phys.* **1995**, *102*, 1461−1462.
(44) Blum, L.; Vericat, F. *J. Phys. Chem.* **1996**, *100*, 1197−1205.
(45) Degrève, L.; Blum, L. *Physica A* **1996**, *224*, 550−557.
(46) Blum, L.; Degreve, L. *Mol. Phys.* **1996**, *88*, 585−590.
(47) Roberts, C. J.; Debenedetti, P. G. *J. Chem. Phys.* **1996**, *105*, 658−672.
(48) Borick, S. S.; Debenedetti, P. G.; Sastry, S. *J. Phys. Chem.* **1995**, 3781−3792.
(49) Besseling, N. A. M.; Scheutjens, J. M. H. M. *J. Phys. Chem.* **1994**, *98*, 11597−11609.
(50) Besseling, N. A. M.; Lyklema, J. *J. Phys. Chem.* **1994**, *98*, 11610−11622.
(51) Dunbrack, R. L.; Silverstein, K. A. T.; Dill, K. A.; Haymet, A. D. J. Unpublished data, 1995.
(52) Bell, G. M. *J. Phys. C.: Solid State Phys.* **1972**, *5*, 889−905.
(53) Allen, M. P.; Tildesley, D. J. *Computer simulation of liquids;* Oxford University Press: Oxford, 1987.

displacements in the coordinates and angle of the chosen molecule. These increments are automatically adjusted during an initial equilibration simulation to achieve approximately a 50% acceptance ratio. To hold the pressure constant, every 5 passes[54] (1 pass = N molecules), an attempt is made to scale the dimensions of the box, and all of its component particles, according to

$$q_i \rightarrow q_i(1 + \xi\Delta q) \tag{6}$$

where the q_i's represent the particle coordinates and box length, and the random number ξ and maximum volume increment Δq are defined as above.

Unless otherwise indicated, all simulations in this study were performed on systems of 60 water molecules (covering the same area as a cross-section of a 3D system having about 500 particles), using standard periodic boundary conditions and the minimum image convention. The starting configuration of each phase point was selected at random, and the first 2×10^4 passes were discarded as the system equilibrated. Statistics were gathered over the next 1×10^7 passes. Simulations with solutes were carried out under the same procedures with 60 water molecules and a single LJ solute (with the same well-depth and contact parameters as the water molecules) fixed in the center of the simulation box.

B. Computational Speed Enhancements. To speed up the hydrogen bond calculation, two computational enhancements were implemented; they have virtually no effect on the Markov chain of states generated. First, an interparticle distance cutoff is chosen, beyond which hydrogen bond energies are assumed to equal zero. The cutoff was chosen such that the energy of neglected interactions does not exceed 1×10^{-10}, corresponding to a distance of $\approx$0.577. We did not use a cutoff for the LJ interaction, other than that implied by the minimum image convention. The second speed-up involves the form of the hydrogen bond calculation. Since the Gaussian-width parameter is so narrow, two arms of one molecule can never make an appreciable interaction with the same neighboring molecule (of course, one arm *can* interact with arms of *different* neighbors, forming a bifurcated hydrogen bond). Therefore, it is unnecessary to calculate all 9 arm−arm interactions for two water molecules. Instead, we predetermine which arm of each molecule is nearest to the intermolecular axis vector, and then calculate only the hydrogen bond between the appropriate two arms. This is accomplished with the following simple formula, and speeds up the total simulation time by roughly a factor of 2:

$$U_{\mathrm{HB}}(\boldsymbol{X_i},\boldsymbol{X_j}) = \epsilon_{\mathrm{HB}}\, G(r_{ij} - r_{HB})\, G(u(i,\hat{\boldsymbol{u}}_{ij}) - 1)\, G(v(j,\hat{\boldsymbol{u}}_{ij}) + 1) \tag{7}$$

where the expressions,

$$u(i,\hat{\boldsymbol{u}}_{ij}) = \mathrm{MAX}(\hat{\boldsymbol{i}}_1\cdot\hat{\boldsymbol{u}}_{ij},\hat{\boldsymbol{i}}_2\cdot\hat{\boldsymbol{u}}_{ij},\hat{\boldsymbol{i}}_3\cdot\hat{\boldsymbol{u}}_{ij})$$

$$v(j,\hat{\boldsymbol{u}}_{ij}) = \mathrm{MIN}(\hat{\boldsymbol{j}}_1\cdot\hat{\boldsymbol{u}}_{ij},\hat{\boldsymbol{j}}_2\cdot\hat{\boldsymbol{u}}_{ij},\hat{\boldsymbol{j}}_3\cdot\hat{\boldsymbol{u}}_{ij}) \tag{8}$$

select out the appropriate arm of the ith and jth molecule, respectively, and the Gaussian function, $G(x)$, again has the form defined in eq 4.

Most of the simulation runs were performed on the farm of DEC Alphas at the University of Sydney, requiring approximately 30 h of CPU time per phase point. A comparable study (i.e., with error bars of the same size) on a 3D model would take approximately 2 orders of magnitude longer, due to the number of particles that would be needed.

C. Calculations of Thermodynamic Quantities. Mechanical averages such as the enthalpy and volume are computed in the standard way, as the average of those quantities over the course of the simulation. The heat capacity, C_p*, the isothermal compressibility, κ*, and the thermal expansion coefficient, α*, are computed from the fluctuations:

$$C_p^* = \frac{C_p}{k_B} = \frac{\langle H^{*2}\rangle - \langle H^*\rangle^2}{NT^{*2}} \tag{9}$$

$$\kappa^* = \frac{\langle V^{*2}\rangle - \langle V^*\rangle^2}{T^*\langle V^*\rangle} \tag{10}$$

$$\alpha^* = \frac{\langle V^*H^*\rangle - \langle V^*\rangle\langle H^*\rangle}{T^{*2}\langle V^*\rangle} \tag{11}$$

where k_B is the Boltzmann constant.

For the insertion of a model solute into water, all thermodynamic averages were computed with use of the Widom test-particle method[55] and related fluctuation formulas. The Widom method is a specific case of the free energy perturbation technique. A ghost particle is placed at random among the N molecules of the pure fluid, but not allowed to interact. Instead, an appropriately weighted scaling of the solute's hypothetical interaction with the fluid is computed. In this manner, the free energy change and appropriate thermodynamic derivatives can be computed in terms of the configurations generated in the reference pure fluid. In principle, the configurations which contribute strongly to the solution (i.e., the ensemble of $N + 1$ particles) will arise in the reference fluid through fluctuations, and make a significant contribution to the computed thermodynamic values, if the simulation is run long enough. However, in practice, such configurations are never fully explored if the reference ensemble differs greatly from that of the solution (e.g., as in the case of a large solute, where a cavity large enough to accommodate it would never be found in reasonable simulation time[56]). Guillot and Guissani used the Widom method to compute free energies, enthalpies, and entropies at several temperatures for methane and various noble gases.[57,58] Although this was a pioneering study, showing the wide utility of the test-particle method, the transfer entropies and enthalpies were not well converged (judging by the noise in their plots, particularly at low temperature).

The advantage of the test-particle method is that the thermodynamics of transfer can be calculated accurately for small solutes by using only a single simulation; free energy perturbation (FEP) and thermodynamic integration (TI) methods require multiple-step transformations. Also in the Widom method, there are multiple insertion sites in each *snapshot* of the fluid, so several attempted insertions can be made per frame. These two features make the insertion method far superior to both FEP and TI, so long as the solutes inserted are small. As a check, we compared our test-particle results with those calculated with FEP and TI at a few temperatures, and obtained nearly-perfect agreement. In the Appendix, we collect together the appropriate test-particle equations for computing transfer free energies, enthalpies, entropies, molar volumes, and heat capacities.

(54) Jorgensen, W. L. *Chem. Phys. Lett.* **1982**, *92*, 405−410.
(55) Widom, B. *J. Chem. Phys.* **1963**, *39*, 2808−2812.
(56) Beutler, T. C.; Béguelin, D. R.; van Gunsteren, W. F. *J. Chem. Phys.* **1995**, *102*, 3787−3793.
(57) Guillot, B.; Guissani, Y.; Bratos, S. *J. Chem. Phys.* **1991**, *95*, 3643−3648.
(58) Guillot, B.; Guissani, Y. *J. Chem. Phys.* **1993**, *99*, 8075−8094.

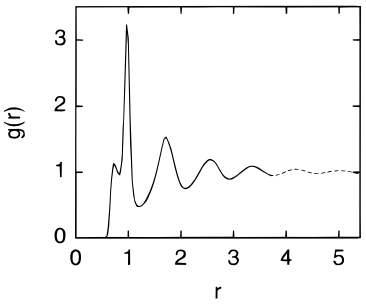

Figure 2. Pair correlation function at $T^* = 0.20$, $P^* = 0.19$ for boxes containing 60 (solid line) and 120 (dashed line) particles overlap exactly. This observed box size insensitivity is representative of other temperatures and pressures studied.

As an additional check, we determined that our simulations are not limited by artifacts of box size. We found no dependence of the thermodynamic properties on the size or shape of the simulation box. For a few state points, simulations were carried out with 120 water molecules, to compare with the usual 60. Figure 2 shows a typical comparison of the pair correlation function for the two box sizes. All thermodynamic values are identical within the error bars.

4. Results for Bulk Water

MB Water Captures Some Experimentally Observed Properties of Real Water. Constant-pressure simulations of pure MB water at a reduced pressure of 0.19 reveal several similarities to pure water. Trends at a lower pressure of 0.12 were also explored, and had all of the same qualitative trends, except for a more poorly defined minimum in the isothermal compressibility. A limitation of our study, as with many others, is that we do not know the full phase diagram,[59] but the part we have explored is sketched in Figure 1 of ref 60.

MB Water Freezes into an Ice-like Structure at Low Temperatures. At low temperatures, MB water has a nonclose packed ice-like ground state, having low density and crystalline ordering. The hexagonal symmetry is the same as would be observed in real 3D ice, viewed down the *c*-axis. MB ice forms spontaneously from a random initial state in constant pressure MC simulations.[61] An ice configuration is shown in Figure 3, along with a typical fluid configuration, for which there is considerably less regularity. As with real water, MB ice has lower density than MB liquid water. In the MB model, the lower density of ice arises because the hydrogen-bonding interactions that favor low-density ordered packing are stronger than the van der Waals interactions that favor random higher-density packing.

The Liquid Is Denser Than the Ice Phase. As noted above, MB ice has an open, low-density structure. The ice structure is a result of the optimization of hydrogen bonding. Heating melts the ice, leading to a liquid of higher density than the solid, indicating that MB ice would float on its liquid, just as real water does. Moreover, it follows from the Clapeyron equation, $dp/dT = \Delta S/\Delta V$, that since the molar volume is lower in the phase of higher entropy (assumed to be the liquid), the liquid/solid-phase boundary will have the typical "backward" slope that water has, $dp/dT < 0$, whereby the melting pressure decreases with temperature. The thermal expansion coefficient, $\alpha = 1/V(\partial V/\partial T)_P$ shown in Figure 4c, is just the derivative of the function in Figure 4a. As in real water, the thermal expansion coefficient becomes negative at low temperature, and equals zero at the density anomaly temperature.

The Density Anomaly. If liquid water is heated above its melting temperature, a remarkable behavior is observed: the density at first *increases*, then ultimately decreases as in more normal liquids. The temperature at which the density trend changes from increasing to decreasing is the density anomaly, or temperature of maximum density (TMD). Figure 4 shows that MB water has a density anomaly similar to that of real water.

What is the physical basis for these properties? The MB model gives the following interpretation. The structure and thermodynamics of the ice phase is dominated by hydrogen bonding. The relatively low density of ice is due to the fact that hydrogen bonding is stronger than the van der Waals interactions. Optimal hydrogen bonding is incommensurate with the tighter packing that would be favored by the van der Waals interactions. Ice melts when the thermal energy is sufficient to disrupt and disorder the hydrogen bonds, broadening the distribution of H-bond angles and lengths. Now among this broadened H-bond distribution, the van der Waals interactions favor those conformations of the system that have higher density. Hence liquid water is denser than ice. Heating liquid water continues to further deform hydrogen bonds and increase the density up to the density anomaly temperature. Further increase of temperature beyond the density anomaly weakens both H bonds and van der Waals bonds, thus reducing the density, as in simpler liquids.

The compressibility correlates loosely with density. As the density increases, the molecules are better packed and the compressibility decreases. As bonds break (both hydrogen bonds and van der Waals interactions) with increasing temperature, the fluid density decreases and compressibility increases. Hence just as there is a maximum in the density, there is also a minimum in compressibility.

An alternative explanation of the density anomaly is due to Stillinger.[3] He explains the density anomaly in terms of the shift from ice-like six-membered H-bonded rings toward more strained H-bonded ring networks. Robinson and co-workers[6,62] gave a related explanation: hydrogen-bond bending promotes the crowding of second and more distant neighbors. These may all be different perspectives on the same physics. It may be that different diagnostics report consequences of the same shifted balance between H bonds and van der Waals interactions.

Pure Water Has a High Heat Capacity. Water has an unusually high heat capacity. MB water also has a high heat capacity, of approximately the correct magnitude ($\approx$12 cal mol^{-1} °C^{-1} at its peak, for the configurational component). Moreover, the temperature dependence of the heat capacity of MB water is similar to that found experimentally (see Figure 4e). MB

(59) We believe the liquid range of MB water is probably small and it is possible that the pressure we have chosen to show for the calculations here may be above the critical pressure.[60] But even if this is the case, this does not limit the value of the model for the properties we study here.

(60) Silverstein, K. A. T.; Dill, K. A.; Haymet, A. D. J. Hydrophobicity in a simple model of water: solvation and hydrogen bond energies. *Fluid Phase Equilibria*. In press.

(61) Note, however, that the "ice" that forms in a square box is *not* of the lowest-energy possible in the model. A perfect honeycomb lattice of $a \times b$ molecules fits in a rectangular unit cell of sides $(3a/2) \times (b\sqrt{3}/2)$, where a and b are both even; so a square will stretch the hydrogen bonds along one of the coordinate axes, to retain the periodicity through the boundaries. Hence in representing ice in this model accurately, one should begin with a rectangular box of the proper dimensions. But the shape of the box has absolutely no effect on the converged properties of the simulations for disordered fluid states, which is the state of interest here.

(62) Cho, C. H.; Singh,; Robinson, G. W. *Phys. Rev. Lett.* **1996**, *76*, 1651−1654.

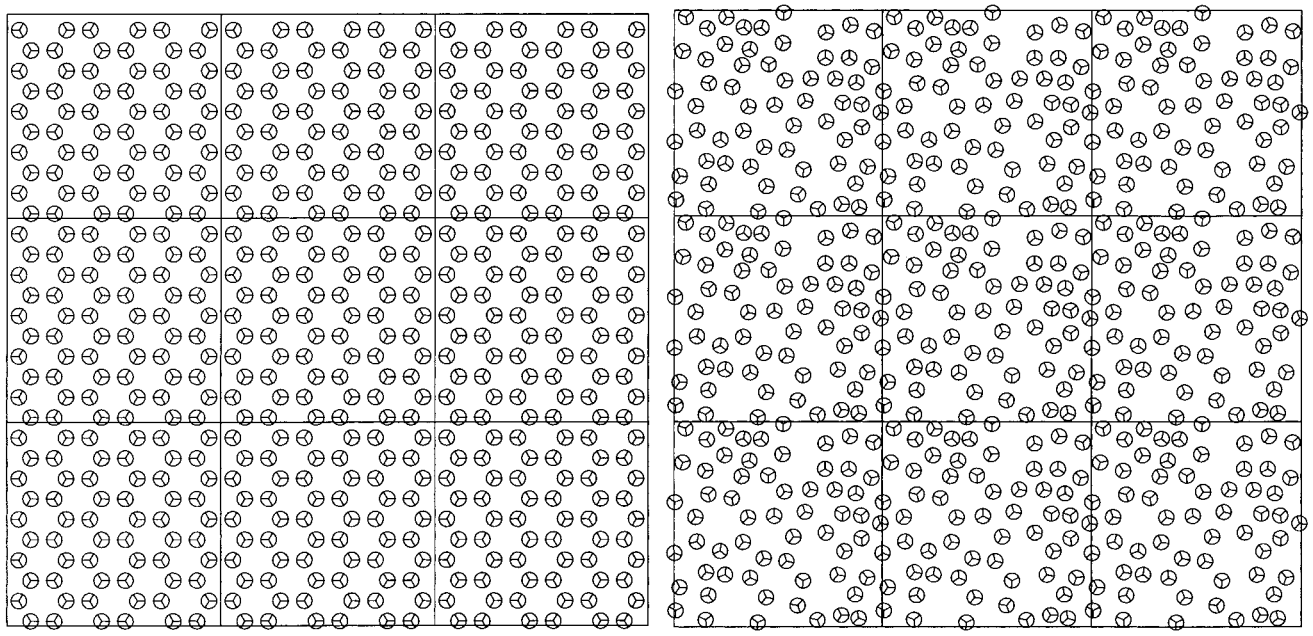

Figure 3. Two snapshots of a system of 60 MB water molecules: on the left, the ground-state "ice" configuration forms a perfect hexagonal honeycomb lattice; and on the right, a typical liquid configuration at $T^* = 0.20$, $\rho = 0.9$.

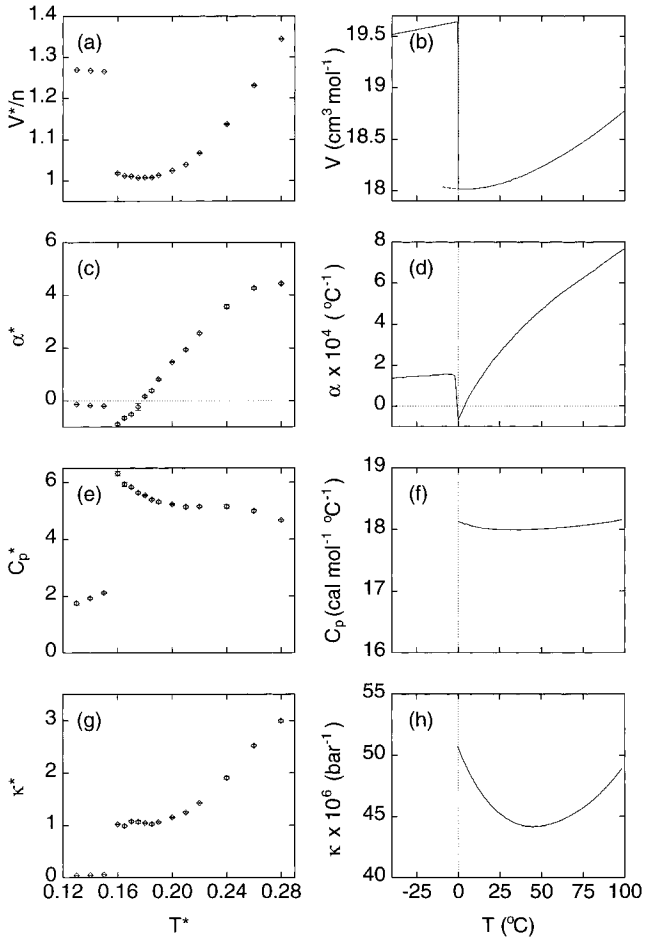

Figure 4. Comparison of various simulated temperature trends in pure MB water (a, c, e, and g) and experiment (b, d, f, and h). Experimental data are replotted from ref 1: molar volumes, (a) and (b); thermal expansion coefficient, (c) and (d); heat capacity (e) and (f); and isothermal compressibility, (g) and (h). Simulated quantities are in reduced units, as described in the text ($T^* = k_BT/|\epsilon_{HB}|$, $V^* = V/r_{HB}^2$, and pressure is defined so that $P^*V^* = PV/|\epsilon_{HB}|$). Error bars reported throughout this work are one standard deviation about the mean.

water has a minimum in the isothermal compressibility vs temperature, but it is not as pronounced as in experiments (see Figure 4g).

What accounts for the heat capacity of pure water? Since the heat capacity is defined as $C_p = (\partial H/\partial T)_P$, the heat capacity describes the extent to which some kind of bonds are broken (increasing H) with increasing temperature. Breaking bonds is an energy storage mechanism. The heat capacity is low in the ice phase because thermal energy at those temperatures is too small to disrupt the H bonds. The heat capacity peaks at the melting temperature where the solid-like H bonds of ice are weakened to become the liquid-like H bonds of liquid water. The reason liquid water has a higher heat capacity than van der Waals liquids have is because water has an additional energy storage mechanism, namely the H bonds, that can also be disrupted by thermal energies.

5. Results for a Single Solute Molecule in Water

The Thermal Anomalies of the Hydrophobic Effect Are Also Found in MB Water. To study the transfer of hydrophobic solutes into MB water, we performed separate MC simulations for the pure fluid and the fluid with a single fixed nonpolar LJ solute (with the same parameters as their water counterparts) under various external conditions. Thermodynamic quantities were obtained from the Widom test-particle method, as described earlier and in the Appendix. Structural distributions were obtained directly from the simulated dilute solutions.

We find that MB water as a solvent is much like real water in its thermal behavior. Figure 5 shows a comparison of the model thermodynamics to the corresponding experimental values[63] for the transfer of gaseous argon into water. The experimental data were obtained from Crovetto et al.,[64] using the Ben-Naim standard state,[65] and from Biggerstaff and

(63) Note that the experimental data were obtained along the liquid−vapor coexistence curve, whereas our data are at constant pressure.

(64) Crovetto, R.; Fernández Prini, R.; Japas, M. L. *J. Chem. Phys.* **1982**, *76*, 1077−1086.

(65) Ben-Naim, A. *Solvation Thermodynamics;* Plenum Press: New York, 1987.

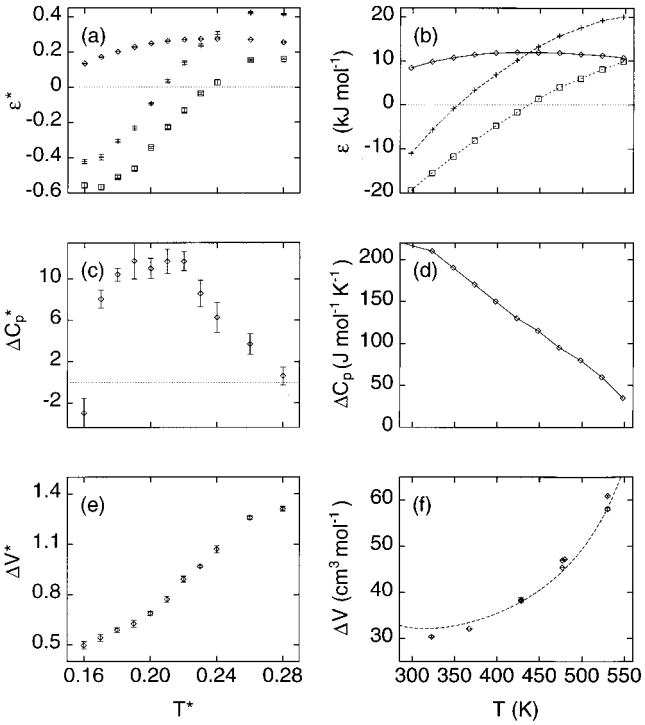

Figure 5. Temperature trends in the transfer thermodynamics of a simple LJ solute in MB water (a, c, e), as compared to the experimental transfer of gaseous Ar into water (b, d, f). (a) Simulation data (this work) for ΔG_{tr} (diamonds), ΔH_{tr} (plus signs), and $T\Delta S_{tr}$ (squares) and for (b) experiments (originally reported in ref 64, and adjusted for the Ben-Naim standard state in ref 65) for the same quantities. The large positive heat capacities of transfer are shown in (c) for this work and (d) from the same experimental source. Also shown are the apparent molar volumes of transfer for (e) simulations and (f) the experiments of Biggerstaff and Wood (ref 66) (symbols) replotted along with the analytical infinite-dilution expression of Harvey et al.[84] (line).

Wood.[66] The correct temperature trends of the free energy, enthalpy, and entropy of transfer are given by the model, as shown in Figure 5a,b. Hence the defining features of the hydrophobic effect are captured by the MB model: The large temperature dependence of the transfer enthalpy and entropy (and the curvature in the free energy) all indicate that the heat capacity is quite large. Indeed, we have calculated the heat capacity of transfer, shown in Figure 5c alongside its experimental counterpart in Figure 5d, and it is large and positive, declining with increasing temperature. Finally, the molar volume of transfer is also plotted in Figure 5. It is interesting to note that, consistent with experiments, the slope of this curve is considerably steeper than that in Figure 4a for pure water. That is, increasing temperature opens up more space around the solute than around water molecules.

The solute−water pair correlation function $g_{SW}(r)$ is shown in Figure 6. It flattens out with increasing temperature. However, it is unclear how much of this effect is actually induced by the solute per se, and how much is merely a reflection of the natural breakdown of bulk water structure with temperature.

To analyze the water behavior in the shells around the solute, we define the first and second shells of water molecules as those within the first and second minima of $g_{SW}(r)$, respectively. We analyze the angular distributions of water molecules in each shell. Figure 7a shows that at low temperature, the water

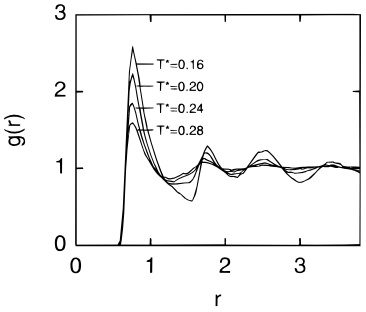

Figure 6. Solute−water pair correlation function at the four temperatures indicated in the figure.

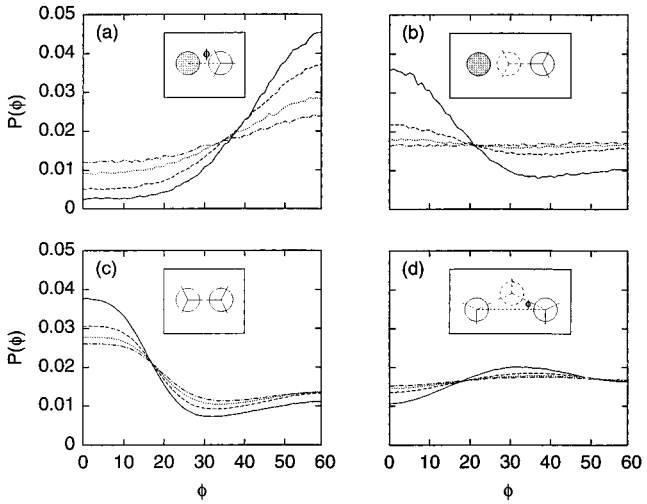

Figure 7. Angular distributions of (a) first shell and (b) second shell water molecules about the solute, in comparison to the (c) first and (d) second shell neighbors of bulk water molecules at four temperatures: $T^* = 0.16$ (solid), 0.20 (dashed), 0.24 (dotted), and 0.28 (dot-dashed). The most-probable orientations are shown in the insets. The angle ϕ, measured in degrees, is the angle that the closest arm of the neighboring (rightmost) water molecule makes with the line connecting its center to the center of the reference (leftmost) molecule. $P(\phi)$ indicates the fraction of molecules observed in 1° bins about ϕ.

molecules "straddle" the solute, to avoid wasting hydrogen bonds, consistent with observations of other simulation models.[67,68] We also observe that this angular order diminishes rapidly with temperature, particularly for those water molecules in the second shell (see Figure 7b). A similar structural breakdown with increasing temperature was inferred from pair correlation functions by Guillot and Guissani.[58]

Now we consider the water−water relationship. The first and second neighbors of bulk and shell water molecules are defined as those molecules that are within the first and second minima of $g_{WW}(r)$, the water−water pair correlation function. At low temperature, $g_{WW}(r)$ for the first-shell water molecules is remarkably similar to that of bulk water, despite the excluded volume of the nearby solute (see Figure 6 in ref 60). The significance of this observation was discussed by Hirata and Rossky,[69] where references to several 3D studies making the same observation can also be found. We also find that the orientational ordering of water molecules surrounding the solute is *more* pronounced than that observed around bulk water molecules (see Figure 7, parts c and d in contrast to parts a and

(66) Biggerstaff, D. R.; Wood, R. H. *J. Phys. Chem.* **1988**, *92*, 1988−1994.

(67) Geiger, A.; Rahman, A.; Stillinger, F. H. *J. Chem. Phys.* **1979**, *70*, 263−276.

(68) Mancera, R. L.; Buckingham, A. D. *J. Phys. Chem.* **1995**, *99*, 14632−14640.

(69) Hirata, F.; Rossky, P. J. *J. Chem. Phys.* **1981**, *74*, 5324−5326.

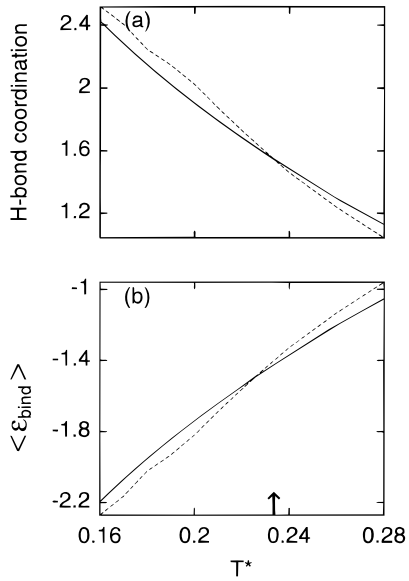

Figure 8. (a) Average hydrogen bond coordination and (b) binding energy of shell (dashed) and bulk (solid) water molecules. The arrow indicates T_S in the model.

b). Furthermore, Figure 7 shows that the angular ordering around the solute is more temperature sensitive than that around a bulk water molecule.

The importance of orientational ordering in this study at first appears to be at odds with recent studies by Head-Gordon.[70,71] Using an orientationally isotropic reference fluid[72,73] which resembles water only in its OO pair correlation function, she showed that the energetics of association of two methane molecules can be quantitatively obtained in the absence of angular ordering. Other studies also have successfully reproduced these and other characteristics of hydrophobicity,[74−76] despite omitting all angular information. The discrepancy may reside in a cancellation of errors in which an overestimate in the entropy cost at the pair-correlation level is canceled by the omitted restrictions in angular degrees of freedom.[77]

The Entropy Convergence Temperature, T_S, Is the Point at Which Shell and Bulk Waters around a Solute Reverse Roles in Hydrogen Bonding. As in real water, the MB model has a temperature T_S at which the entropy of transfer of the nonpolar solute is zero,[9,25,78] i.e., $T_S\ \Delta S_{tr} = 0$. What is the physical basis for T_S? In the MB model, this temperature delineates two different behaviors of shell water molecules around a solute. Below T_S, shell water molecules have more and tighter H bonds than bulk water molecules have (see Figure 8). Above T_S, this behavior reverses: bulk water molecules have more and tighter H bonds than shell water molecules have.

In Figure 8, hydrogen bond coordination around a given molecule was calculated by summing all of its pairwise hydrogen bond interactions that are below an energetic cutoff. Several cutoffs (in the range from −0.5 to −0.25) were explored yielding the same crossing temperature and qualitative temperature trends. The binding energy is defined to be the sum of the energetic interactions of a given water with all other water molecules in the simulation. (To be fair in making conclusions about relative structuring, the interaction with the solute is left out.) From either measure, it is clear that the shell molecules have more favorable energies and higher hydrogen bond coordination than bulk water molecules below T_S. Beyond this temperature, the roles reverse. The widths of both coordination number and binding energy distributions are tighter at all temperatures for shell molecules (not shown).

Though recent computational studies have provided little evidence for significant structuring in the shell,[10] it should be noted that these studies are done at room temperature, and that the most significant structuring in our study occurs at low temperatures just above freezing. Since at high temperatures the shell has a net *disruption* of H bonds relative to the bulk, our observations are not inconsistent with the more realistic studies for the intervening temperatures.

At all temperatures we studied, the water molecules directly surrounding shell molecules have more orientational order than those around bulk water molecules. Second-neighbor water molecules around shell-water molecules have only slight ordering up to T_S (Figure 7 in ref 60).

Why should shell water molecules be more ordered and have better H-bond coordination than bulk water molecules? Matubayasi has proposed a geometric explanation.[79] He showed that a solute adjacent to two shell molecules occupies a region of space that is inconsistent with local solvent tetrahedrality (i.e. in reference to the angle a third solvent molecule might make with the pair). Thus, inserting the solute increases the probability of local tetrahedrality among the water molecules (since solvent molecules will not be in the occluded "mismatching" zone). Better tetrahedrality correlates with better hydrogen bonding arrangements. This explanation, invoking 3- and 4-body correlations, may be important, but it is insufficient to explain T_S and the reversal of shell and bulk H bonding we observe at higher temperatures. We believe such geometric arguments may be part of the explanation for hydrophobicity, but not all of it.

Care should be taken not to confuse T_S, the temperature at which the transfer entropy is zero, with T_S*,[78,80] where the transfer entropy of various solutes converge (i.e., the so-called convergence temperature). The two temperatures are nearly identical only for liguid → water transfers, and not for the gas → water transfers in this work. A recent statistical mechanical theory for the convergence temperature, T_S*, has been proposed by Garde et al.,[81] using the theory of Hummer et al.[75,76] These authors have used an information theory model that tracks the fluctuations of void volumes in standard simulated water models, and have linked T_S* to the relative temperature insensitivity of water's isothermal compressibility as compared to simple liquids.

Inserting a Nonpolar Solute Also Inserts Local Free Volume. To study molar volumes of transfer and ideas of clathration, we use Voronoi polygons. A Voronoi polygon defines the region of space that is closer to a given molecule than to any other molecule in the system. Thus, the volume of the polygon is a direct measure of the local "space" attributable to each molecule. The number of edges in these polygons gives a geometric measure of coordination.

(70) Head-Gordon, T. *Chem. Phys. Lett.* **1994**, *227*, 215−220.
(71) Head-Gordon, T. *J. Am. Chem. Soc.* **1995**, *117*, 501−507.
(72) Head-Gordon, T.; Stillinger, F. H. *J. Chem. Phys.* **1993**, *98*, 3313−3327.
(73) Stillinger, F. H.; Head-Gordon, T. *Phys. Rev. E* **1993**, *47*, 2484−2490.
(74) Pratt, L. R.; Chandler, D. *J. Chem. Phys.* **1977**, *67*, 3683−3704.
(75) Hummer, G.; Garde, S.; García, A. E.; Pohorille, A.; Pratt, L. R. *Proc. Natl. Acad. Sci. U.S.A.* **1996**, *93*, 8951−8955.
(76) Berne, B. J. *Proc. Natl. Acad. Sci. U.S.A.* **1996**, *93*, 8800−8803.
(77) Silverstein, K. A. T.; Dill, K. A.; Haymet, A. D. J. In preparation.
(78) Baldwin, R. L. *Proc. Natl. Acad. Sci. U.S.A.* **1986**, *83*, 8069−8072.
(79) Matubayasi, N. *J. Am. Chem. Soc.* **1994**, *116*, 1450−1456.
(80) Lee, B. *Proc. Natl. Acad. Sci. U.S.A.* **1991**, *88*, 5154−5158.
(81) Garde, S.; Hummer, G.; García, A. E.; Paulaitis, M. E.; Pratt, L. R. *Phys. Rev. Lett.* **1996**, *77*, 4966−4968.

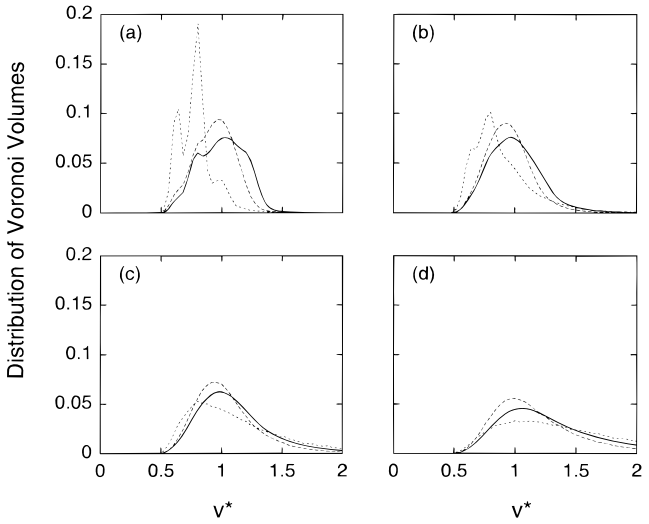

Figure 9. Voronoi volume distributions around bulk water molecules (solid), shell water molecules (dashed), and the solute (dotted) for (a) $T^* = 0.16$, (b) 0.20, (c) 0.24, and (d) 0.28. Here, v^* denotes the reduced volume ($v^* = v/r_{HB}^2$) of a Voronoi polygon, and the *y*-axis measures the relative distributions of Voronoi volumes using a binwidth of 0.04.

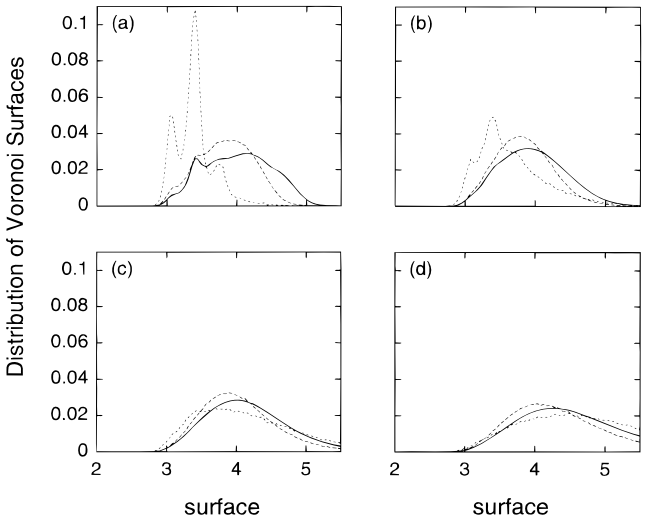

Figure 10. Voronoi surface (perimeter) distributions around bulk water molecules (solid), shell water molecules (dashed), and the solute (dotted) for (a) $T^* = 0.16$, (b) 0.20, (c) 0.24, and (d) 0.28. Voronoi surfaces are in units of r_{HB}, and the *y*-axis measures their relative distributions using a binwidth of 0.04.

The distributions in Voronoi volumes and surfaces (actually perimeters in 2D) around the shell water molecules, bulk water molecules, and solute are shown in Figures 9 and 10, respectively. The average volume, surface, and coordination are shown in Figure 11 as functions of temperature. The model shows that the molar volume of the solute increases with temperature. This increased volume is largely localized around the solute, consistent with the findings of Guillot and Guissani.[58] The average number of water neighbors around a solute increases with temperature, while the average number of water neighbors around a shell water molecule decreases with temperature. This information, taken together with the breadth of the distributions around the solute, suggests that well-ordered small collections of water molecules at low temperature are replaced by highly variable fluctuating larger structures at higher temperatures. The difference between shell and bulk local volumes remains fairly constant over the temperature range.

The Voronoi volumes and surfaces surrounding the solute

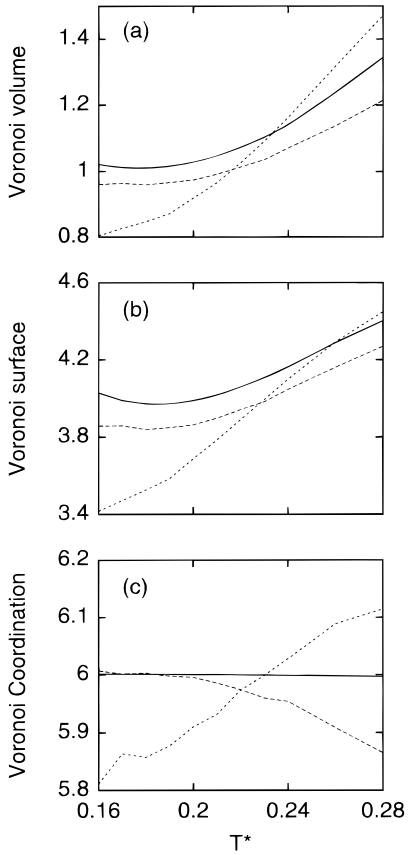

Figure 11. Average Voronoi (a) volume, (b) surface, and (c) coordination for bulk water molecules (solid), shell water molecules (dashed), and the solute (dotted).

Table 1. Computed Voronoi Volumes and Surfaces (perimeters) of Idealized Rings of Water Molecules Surrounding a Solute

ring size	volume	surface
5	0.657	3.09
6	0.866	3.46
7	1.12	3.88

give some indication of clathrate-like populations. We calculated the volumes and surfaces for idealized 5-, 6-, and 7-membered rings of H-bonded water molecules around a solute (see Table 1). The three peaks in the Voronoi distribution curves at the lowest temperature coincide with these idealized values, indicating multiple modes of clathration around the solute, as has been found in 3D studies.[82,83] These peaks weaken with temperature.

6. Conclusions

Our aim has been to model the qualitative thermodynamic trends that characterize water and the hydrophobic effect. We use a simple two-dimensional model of water that describes a competition between Lennard-Jones interactions that favor random dense states and hydrogen bonding that favors ordered open states. At low temperature, MB model water freezes to a low-density crystal, like ice. The anomalous properties of the volume of water with temperature are reproduced: (1) that the liquid state is more dense, and (2) that there is a temperature of maximum density in the liquid range, also known as the density anomaly.

(82) Alagona, G.; Tani, A. *J. Chem. Phys.* **1980**, *72*, 580−588.
(83) Head-Gordon, T. *Proc. Natl. Acad. Sci. U.S.A.* **1995**, *92*, 8308−8312.
(84) Harvey, A. H.; Sengers, J. M. H. L.; Tanger, J. C., IV *J. Phys. Chem.* **1991**, *95*, 932−937.

The MB model reproduces the thermal anomalies of nonpolar solvation, including a large free energy that opposes the insertion of oil into water, a large entropic component at low temperatures, and a large heat capacity. The MB model supports the classical picture of hydrophobic hydration, in which the orientations of shell water molecules that are restricted at low temperature become accessible upon heating, as summarized by Dill.[23] At low temperature, first-shell water molecules are ordered around small inert solutes and have strengthened hydrogen bonds relative to bulk water molecules. There are multiple interchanging modes of clathration. This excess ordering of the shell causes the transfer enthalpies and entropies to be negative. As temperature is increased, shell water structure melts out at a lower temperature than bulk water structure, consistent with the assumptions of the two-state model of Muller.[25] The MB model has a temperature T_S at which the transfer entropy changes sign. T_S coincides with the point where the hydrogen bonds in shell and bulk molecules reverse their relative strengths and numbers. Mancera and Buckingham[68] found similar changes in hydrogen-bonding coordination as temperature is increased.

Finally, the steady increase in the molar volume of transfer with temperature is linked to an increase in the local volume surrounding the solute. This occurs as a relatively small number of ordered shell-water motifs give way to more-varied and larger fluctuating structural arrangements.

Acknowledgment. K.A.T.S. gratefully acknowledges support under a U.S. National Science Foundation Graduate Research Fellowship and a UCSF Regent's Fellowship. In Australia, this research was supported by the Australian Research Council (ARC) (Grant No. A29530010), and SydCom, the USyd/UTS Distributed Computing Facility funded by an ARC infrastructure grant. In addition, we would like to thank Karen Tang for her continuous support to K.A.T.S. and helpful suggestions; Mike Laskowski, for his enthusiasm in the early stages of the project; Thomas Beutler, for his advice and simulation tips; and David Agard, Robert Fletterick, Peter Kahn, Peter Kollman, I. D. Kuntz, Ron Siegel, and David Spellmeyer, for helpful discussions on the model.

Appendix: Test-Particle Equations

The main formula pertaining to the test-particle method for computing the transfer free energy is:

$$\Delta G_{tr} = -\ln \langle \exp(-\beta\epsilon) \rangle_N \tag{12}$$

where ϵ is the interaction energy of the ghost particle with the surrounding solvent, $\beta = 1/k_B T$, where k_B is Boltzmann's constant and T is the temperature, and the average is performed over the pure reference fluid. The transfer enthalpy is

$$\Delta H_{tr} = \frac{\langle H_{N+1} \exp(-\beta\epsilon) \rangle_N}{\langle \exp(-\beta\epsilon) \rangle_N} - \langle H_N \rangle_N \tag{13}$$

where H_N is the enthalpy of the pure solvent and $H_{N+1} = H_N + \epsilon$. The corresponding entropy of transfer is therefore

$$T\Delta S_{tr} = \frac{\langle H_{N+1} \exp(-\beta\epsilon) \rangle_N}{\langle \exp(-\beta\epsilon) \rangle_N} - \langle H_N \rangle_N + \ln \langle \exp(-\beta\epsilon) \rangle_N \tag{14}$$

The molar volume of transfer and the heat capacity can be expressed as

$$\Delta V_{tr} = \frac{\langle V \exp(-\beta\epsilon) \rangle_N}{\langle \exp(-\beta\epsilon) \rangle_N} - \langle V \rangle_N \tag{15}$$

and

$$\Delta C_{p,tr} = \frac{\langle H_{N+1}^2 \exp(-\beta\epsilon) \rangle_N}{\langle \exp(-\beta\epsilon) \rangle_N} - \frac{\langle H_{N+1} \exp(-\beta\epsilon) \rangle_N^2}{\langle \exp(-\beta\epsilon) \rangle_N} - \langle H_N^2 \rangle_N + \langle H_N \rangle_N^2 \tag{16}$$

respectively.

JA973029K